AMERICAN SOCIETY FOR MICROBIOLOGY | Microbiology Spectrum

| Genetics and Molecular Biology | Research Article

Small protein mediates inhibition of ammonium transport in *Methanosarcina mazei*—an ancient mechanism?

Tim Habenicht,[1] Katrin Weidenbach,[1] Adrian Velazquez-Campoy,[2,3,4,5] Ruben M. Buey,[6] Monica Balsera,[7] Ruth A. Schmitz[1]

AUTHOR AFFILIATIONS See affiliation list on p. 14.

ABSTRACT In the past decade, small open reading frames (sORFs) coding for proteins less than 70 amino acids (aa) in length have moved into the focus of science. sORFs and the corresponding small proteins have been recently identified in all three domains of life. However, the majority of small proteins remain functionally uncharacterized. While several bacterial small proteins have already been described, the number of identified and functionally characterized small proteins in archaea is still limited. In this study, we have discovered that the small protein 36 (sP36), which consists of only 61 aa, plays a critical role in regulating nitrogen metabolism in *Methanosarcina mazei*. The absence of sP36 significantly delays the growth of *M. mazei* when transitioning from nitrogen limitation to nitrogen sufficiency, as compared to the wild type. Through our *in vivo* experiments, we have observed that during nitrogen limitation, sP36 is dispersed throughout the cytoplasm; however, upon shifting the cells to nitrogen sufficiency, it relocates to the cytoplasmic membrane. Furthermore, an *in vitro* biochemical analysis clearly showed that sP36 interacts with high affinity with the ammonium transporter $AmtB_1$ present in the cytoplasmic membrane during nitrogen limitation as well as with the PII-like protein $GlnK_1$. Moreover, the *in vivo* $GlnK_1$ interaction with $AmtB_1$ due to nitrogen upshifts requires the presence of sP36. Based on our findings, we propose that in response to an ammonium upshift, sP36 targets the ammonium transporter $AmtB_1$ and inhibits its activity by mediating the interaction with $GlnK_1$.

IMPORTANCE Small proteins containing fewer than 70 amino acids, which were previously disregarded due to computational prediction and biochemical detection challenges, have gained increased attention in the scientific community in recent years. However, the number of functionally characterized small proteins, especially in archaea, is still limited. Here, by using biochemical and genetic approaches, we demonstrate a crucial role of the small protein sP36 in the nitrogen metabolism of *M. mazei*, which modulates the ammonium transporter AmtB1 according to nitrogen availability. This modulation might represent an ancient archaeal mechanism of AmtB1 inhibition, in contrast to the well-studied uridylylation-dependent regulation in bacteria.

KEYWORDS small protein, ammonium transport, protein regulation, pII protein, archaea, membrane proteins

Small proteins are a significant part of the proteome in all organisms across the tree of life. The definition of this class of proteins is based on their small size rather than a functional criterion, which is typically defined by a cutoff ranging from 70 to 100 amino acids (1–5). Unlike peptides produced through posttranslational processing of larger proteins, the small proteins we refer to here are encoded by independent small open reading frames (sORFs). These sORF-encoded proteins, with a length of fewer than 70 amino acids (aa), have been historically overlooked and understudied due to bioinformatic biases inherent in conventional genome annotations and technical challenges

Editor Emily Weinert, The Pennsylvania State University, University Park, Pennsylvania, USA

Address correspondence to Ruth A. Schmitz, rschmitz@ifam.uni-kiel.de.

The authors declare no conflict of interest.

See the funding table on p. 15.

Received 10 July 2023
Accepted 29 September 2023
Published 1 November 2023

associated with classical biochemical approaches, such as SDS-PAGE or mass spectrometry. Conventional gene annotations were primarily designed to identify larger proteins (6, 7), while proteomic tools relied on obtaining multiple peptides of one protein through tryptic digestion, which is often not feasible for small proteins (8). These challenges have impeded the annotation and characterization of small proteins in the past, creating a promising avenue for detailed mechanistic studies and functional analysis today, with high untapped potential.

Genome-wide transcriptomic, translatomic, and proteomic methods have been improved and developed in recent years to address and overcome the challenges of identifying the small proteome. The application of deep-sequencing technologies, as well as improvements and adaptation of ribosome profiling tools to bacteria and archaea, and optimized peptidome analyses by mass spectrometry allowed the identification of a constantly growing number of sORFs and the respective small proteins in bacteria and archaea (9–14). As a result, an increasing number of reports on small proteins encoded by sORFs are currently emerging and their physiological importance has been proven in numerous examples, by participation in various cellular functions such as cell division, transport, and enzymatic processes (3, 15, 16).

Since small proteins have come in the focus of science, it becomes more evident that a significant amount of proteins with less than 70 aa are associated with the cytoplasmic membrane. For *Escherichia coli*, a large portion of identified small proteins were shown to be localized at the membrane, where they might interact with larger proteins and protein complexes such as signal receptors or transporters (17–19). However, archaea exhibit fewer identified small proteins, and functional characterization is limited to a handful of examples, of which only one is part of a transporter (20–23).

Methanosarcina mazei strain Gö1 belongs to the order Methanosarcinales and is strictly anaerobic. This versatile group of methylotrophic archaea can utilize a variety of substrates, including methanol, methylamines, and acetate, in addition to CO_2 and H_2, as a source of both carbon and energy, with the ultimate product being methane, a greenhouse gas (24, 25). In the absence of another suitable nitrogen source, *M. mazei* is able to reduce and fix molecular nitrogen (26). This highly energy-consuming process of nitrogen fixation as well as the general nitrogen metabolism are strictly regulated on transcriptional, posttranscriptional, and posttranslational levels in response to nitrogen availability, which has been studied extensively in recent years (27–33). As known for bacteria, several key components of the nitrogen metabolism are only present and highly expressed under N-starvation, for example, glutamine synthetase, ammonium transporters, diazotrophs, and also nitrogenase (32, 34–37).

Under a sufficient ammonium concentration, nitrogen assimilation in cells occurs through the diffusion of ammonia across the cytoplasmic membrane and its subsequent incorporation into glutamate by glutamate dehydrogenase. However, under conditions of a significantly decreased external ammonium concentration, active transport of ammonium becomes necessary. This transport is facilitated by the trimeric ammonium transporter $AmtB_1$, which is expressed exclusively under nitrogen (N) limitation in *M. mazei* (10, 38) but requires the expenditure of ATP (39, 40). Following transport, ammonium assimilation is facilitated by the glutamine synthetase/GOGAT (glutamine oxoglutarate aminotransferase) system (41). N starvation leads to elevated levels of 2-oxoglutarate (2-OG) within cells, which serves as an internal signal for N starvation (32).

$AmtB_1$ is an ammonium transporter protein of the Amt/Mep/Rh protein family, of which, members can be found in eukaryotes, bacteria, as well as archaea. Through all domains of life, proteins of the Amt family show a highly conserved tertiary structure of 11 transmembrane helices with extracellular N- and cytoplasmic C- terminal domains (42, 43). In *Escherichia coli*, the ammonium transporter AmtB organizes as trimers with each subunit representing a hydrophobic pore for ammonia transport (44–46). The import of NH_4^+ is an energy-consuming process (39, 40). Consequently, the transporter is highly regulated depending on the nitrogen status of the cell to exclude energy dissipation. Based on the structure and complex formation analysis, Coutts et al. (46) showed that in

E. coli, the ammonium transporter is inhibited by a PII-like protein (GlnK) upon a shift to nitrogen sufficiency. This regulation is based on GlnD-dependent deuridylylation of GlnK. The respective *glnK* gene is organized together with the *amtB* gene in an operon (*glnK/amtB*), which is only expressed under nitrogen starvation (47). This coupling of genes encoding an ammonium transporter and a PII-like protein has been identified in most bacteria as well as archaea, indicating a tight functional coexistence (48). However, GlnD, responsible for uridylylation and deuridylylation of GlnK, is not as ubiquitous. Those organisms with a *glnK/amtB* operon but without a *glnD* gene must rely on a different pathway of AmtB regulation.

A large number of potential sORFs were identified in *M. mazei* under N stress conditions through a genome-wide RNA sequencing (RNAseq) analysis (10). Among these, sORF36 encodes a 61 aa protein (sP36) that was confirmed by an LC-MS/MS analysis. Its transcription was shown to increase 2.5-fold under nitrogen limitation, as confirmed at the protein level. Additionally, sORF36 and sP36 are highly conserved on the DNA and protein level, across various archaeal species, suggesting a possible role of sP36 in nitrogen metabolism (31).

In this study, we characterize this additional newly discovered component in nitrogen regulation in *M. mazei*, the small protein sP36 (31). Through genetic and biochemical approaches, we show that sP36 is involved in the adaption to changing nitrogen conditions. Although sP36 does not contain any transmembrane helices, we provide several lines of evidence *in vitro* and *in vivo* that sP36 localizes at the cytoplasmic membrane in response to an ammonium upshift after a period of nitrogen limitation. Using different biochemical approaches, we demonstrated that the observed interaction with the cytoplasmic membrane is the result of the direct interaction between sP36 and the membrane-located ammonium transporter $AmtB_1$. In a pull-down assay, purified His_6-tagged $AmtB_1$, incubated with a native *M. mazei* cell extract, is capable of specifically mediating the retention of chromosomally expressed sP36. Further biochemical analysis demonstrated a high-affinity interaction between sP36 and not only the ammonium transporter $AmtB_1$ but also the regulatory PII-like protein $GlnK_1$.

We propose a plausible model where sP36 acts as an adaptor protein that mediates the $GlnK_1$–$AmtB_1$ interaction to allow a rapid and reversible response to changes in nitrogen availability. This mechanism might represent a more ancient version of the AmtB inhibition by a PII-like protein before the GlnD-dependent uridylylation was developed.

RESULTS

sP36 plays a crucial role during nitrogen upshifts after a period of N limitation

To get insights into the functional role of sP36, a genetic approach was performed. A chromosomal deletion mutant of the respective sORF-encoding sP36 was constructed, replacing the *sORF36* gene with the puromycin-resistance cassette (*pac* cassette) using an allelic replacement approach (see Materials and Methods). The generated mutant strain (*M. mazei* ΔsP36) was verified by Southern blot analysis (Fig. S1). Its growth behavior under different N availabilities was evaluated and compared to the wild type strain (*M. mazei* 3A (wt, selected for improved growth on solid media); Fig. 1). When growing on a minimal medium with ammonium as a sufficient N source (10 mM) or under N limitation (0 mM), no growth phenotype was detectable in the absence of sP36 except that the lag phase was slightly prolonged but reaching identical doubling times. However, when cells were grown under N limitation until early exponential phase (turbidity at 600 nm (T_{600}) = 0.15) and then transferred into fresh ammonium-sufficient media (1.6×10^8 cells in 50 mL media), the cultures of *M. mazei* ΔsP36 showed a significantly prolonged phase of adaptation (38 h lag phase) in the ammonium-sufficient medium, before again entering an exponential growth phase reaching the same doubling time as the wild type. In contrast, the wild type (wt) immediately entered

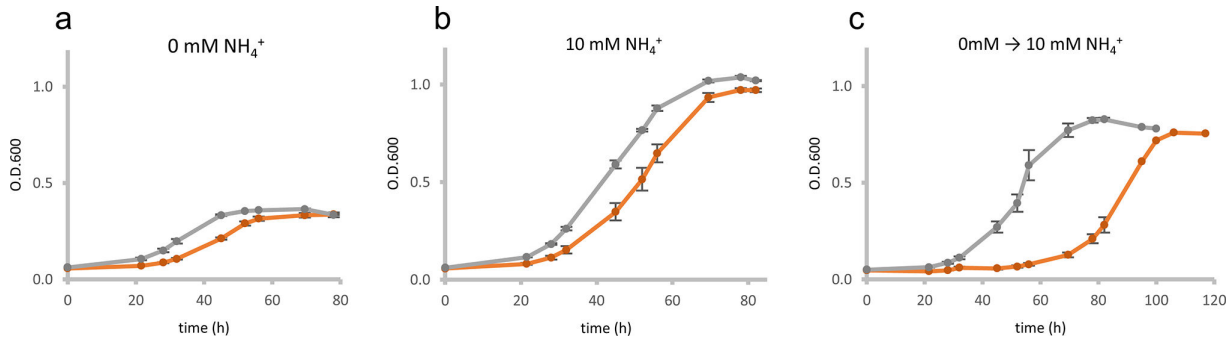

FIG 1 Growth analysis of *M. mazei* ΔsP36 in comparison to *M. mazei* wt: Growth of the *M. mazei* sP36 deletion mutant (ΔsP36), (orange), and the wildtype, (gray), grown under different nitrogen availabilities with either 0 mM (a) or 10 mM (b) NH_4^+ in the medium or shifted from 0 mM to 10 mM (c). The respective NH_4^+ concentration is depicted. In each case, a 50 mL anaerobic minimal medium was inoculated with 1.6×10^8 cells (T_0). The standard deviation of the three biological replicates are shown.

exponential growth after the shift to ammonium sufficiency. These findings strongly indicate the crucial role of sP36 under nitrogen upshift conditions.

We performed a basic local alignment search tool analysis with the *M. mazei* sP36 amino acid sequence (49). Homologs of sP36 were found in a high number of methanogenic and halophilic archaea in seven archaeal families in the two classes of Methanosarcinia and Halobacteria inside the phylum of halobacteriota. Even in the six bacterial families (streptosporangiaceae, propionibacteriaceae, nocardioidaceae, isophaeraceae and one thermoanaerobaculia family), homologs of sP36 were found (see Fig. 2a). Interestingly, those organisms encoding sP36 do not encode a homolog of the uridylyltransferase GlnD, which is required for the uridylyl-dependent AmtB regulation by GlnK, as described in the Introduction. The different homologs of sP36 show 37% to 95% identity on an amino acid level but very high structural conservation based on alphaFold2 (50) predictions (see Fig. 2b).

sP36 localizes at the cytoplasmic membrane in response to a shift from N limitation to N sufficiency

The cellular localization of sP36 under N-limited growth conditions (-N) and after an ammonium upshift was evaluated by subcellular fractionation of the cell extract and subsequent western blot analysis using peptide antibodies directed against sP36. One liter of *M. mazei* cultures were grown under -N. When reaching mid-exponential growth phase (T_{600} = 0.2), 50% of the cultures were shifted to N sufficiency by supplementing with 10 mM ammonium (final concentration). The remaining 50% were kept N-limited. After further incubation for 30 min, subcellular fractionation was conducted as described in Materials and Methods, followed by a western blot analysis of the respective cytoplasmic and membrane fractions using specific peptide antibodies against sP36. Overall, three independent biological replicates were analyzed, each with three technical replicates. Under –N, sP36 was predominantly dispersed in the cytoplasm (93 ±3%). However, upon ammonium upshift, most of sP36 relocated into the membrane fraction (57 ±10%; Fig. 3b). In addition to the shift in localization, there is an apparent change in the molecular weight of the sP36 signal. This change is most likely the result of sP36 oligomerization, which is induced by the shift to increased ammonium concentration *in vivo* or the interaction with a protein in the cytoplasmic membrane.

The observed interaction between sP36 and the cytoplasmic membrane was further verified in an *in vitro* assay using purified tag-less sP36 and cytoplasmic membrane fractions. Membrane fractions from the mutant *M. mazei* strain ΔsP36 grown under -N as well as after an ammonium upshift (+NH_4^+↑) were generated by ultracentrifugation as described in Materials and Methods. The heterologously expressed, purified tag-less sP36 (100 µg) was incubated in the presence of the *M. mazei* ΔsP36 membrane fractions

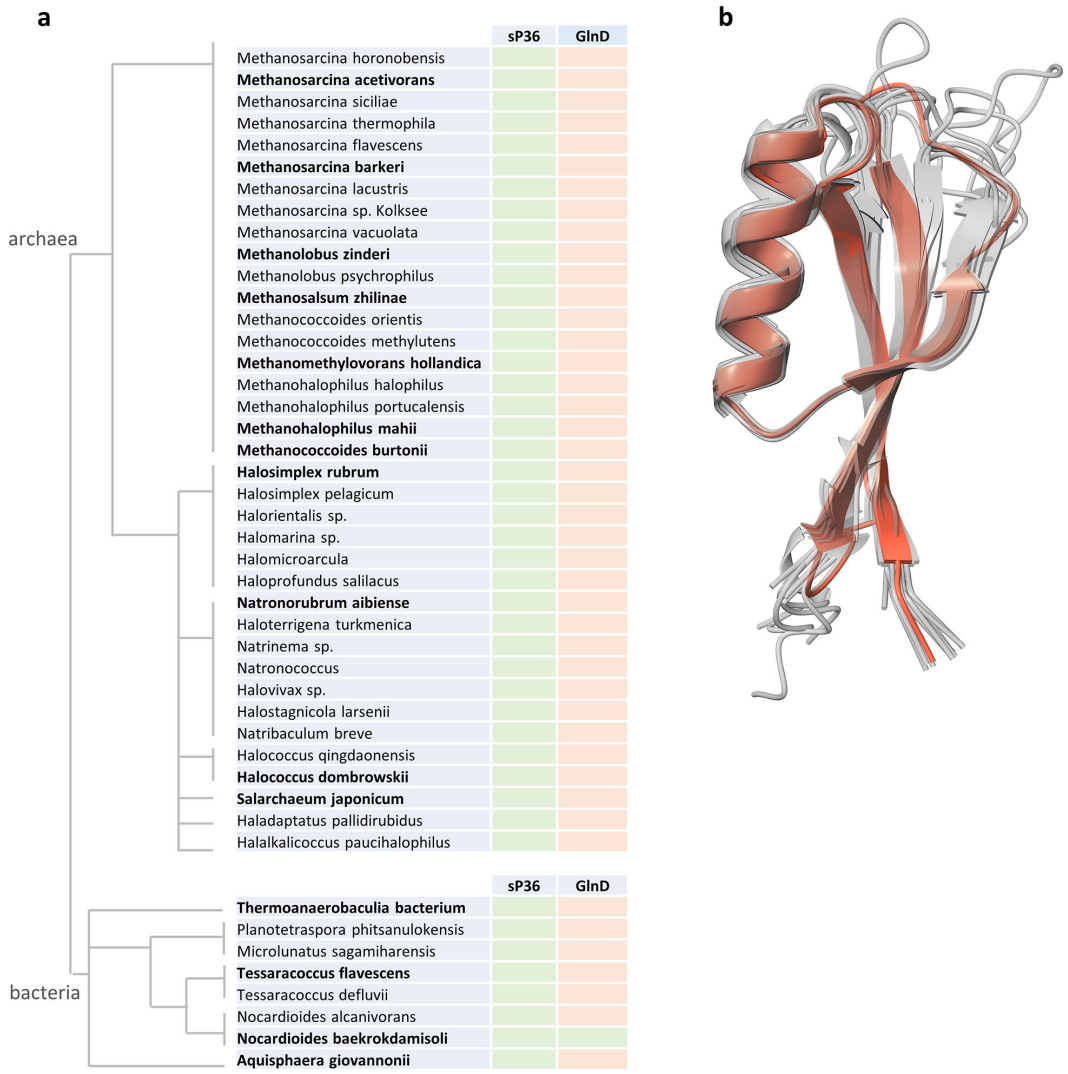

FIG 2 Conservation of sP36. (a) sP36 is conserved in archaea and bacteria. sP36 homologs were found in archaeal and bacterial species. Species which do not encode GlnD are marked in the GlnD column in orange, and those which encode GlnD are marked in green. Taxonomic grouping is based on the Genome Taxonomy Database (51). (b) sP36 structural conservation based on alphaFold2 prediction. sP36 from *M. mazei* is given in yellow. Organisms of which homologs were used for structure predictions are highlighted in bold.

(5 mg) for 15 min at RT (room temperature) followed by ultracentrifugation at 210,000 *g* and 4°C for 1 h. The respective pellet and supernatant were evaluated for the presence of sP36 by western blot analysis using peptide antibodies against sP36 (see Fig. 3c). In the control sample of the *M. mazei* ΔsP36 membrane (-N) without prior incubation with sP36, no signal was detected, neither in the supernatant (lane 6) nor in the membrane fraction (pellet, lane 2), confirming the absence of sP36 in the *M. mazei* ΔsP36 mutant strain as well as the specificity of the antibody. In the absence of membrane fractions, purified sP36 was exclusively present in the supernatant after ultracentrifugation (lane 8 vs lane 4). However, when incubated in the presence of the cytoplasmic membrane fraction of cells grown under nitrogen limitation, approximately 50% of sP36 was detected in the membrane fraction (lane 1, pellet), strongly arguing for a recruiting of the soluble hydrophilic sP36 to the membrane. Even when cells were grown under nitrogen sufficiency, part of the sP36 was detectable in the membrane fraction after centrifugation (lane 3).

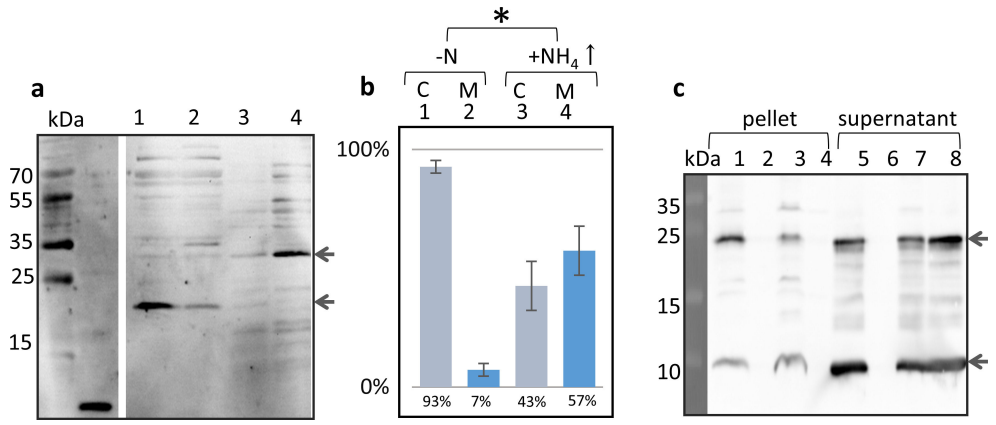

FIG 3 Interaction of sP36 with the cytoplasmic membrane of *M. mazei* under different N conditions. A + B: *M. mazei* cultures were grown under N limitation (0 mM NH_4^+ N_2, (-N). When T_{600} of 0.2 was reached, 50% of the cultures were shifted to N sufficiency (10 mM NH_4^+ final concentration, NH_4). (a) Membrane and the cytoplasmic fractions were analyzed by western blot with a polyclonal antibody raised against sP36. (1) -N cytoplasmic fraction; (2) NH_4 cytoplasmic fraction; (3) -N membrane fraction; and (4) NH_4 membrane fraction. The major sP36 signals are indicated by arrows. Depicted is one exemplary western blot out of three biological replicates. (b) Relative quantification of the dominant bands of sP36 subcellular fractions from *M. mazei*. (1) -N cytoplasmic fraction; (2) -N membrane fraction; (3) NH_4 cytoplasmic fraction; (4) NH_4 membrane fraction; the distribution of the sP36 subcellular localization was calculated based on three biological replicates. The amount of sP36 in the cytoplasm and the membrane fraction of one culture was set to 100%. Significance was tested using the two-tailed *t*-test. *$P = 0.014$; df = 4. (c) *In vitro* interaction of sP36 with *M. mazei* ΔsP36 membrane fractions: untagged sP36 (100 µg derived from His_6-SUMO-sP36) was incubated together with the membrane fraction of *M. mazei* ΔsP36 subcellular fractionation. Lanes 1–4: pellet of 210,000 *g* centrifugation; lane 1: sP36 incubated with the –N membrane fraction of *M. mazei* ΔsP36; lane 2: -N membrane fraction of *M. mazei* ΔsP36 without sP36 (control); lane 3: sP36 incubated with the membrane fraction of *M. mazei* ΔsP36 grown under N sufficiency (+N); lane 4: pellet of sP36 without membrane fraction (control); lanes 5–8: supernatant of 210,000 *g* centrifugation; lane 5: sP36 incubated with the -N membrane fraction of *M. mazei* ΔsP36; lane 6: -N membrane fraction of *M. mazei* ΔsP36 without sP36 (control); lane 7: sP36 incubated with the membrane fraction of *M. mazei* ΔsP36 grown under N sufficiency (10 mM); lane 8: sP36 without membrane fraction (control). The major sP36 signals are indicated by arrows. Depicted is one exemplary western blot out of three biological replicates.

sP36 interacts with ammonium transport proteins

The subcellular localization experiments as shown above strongly suggest localization of sP36 to the cytoplasmatic membrane upon an ammonium upshift. One potential interacting partner of sP36 in the cytoplasmic membrane is the ammonium transporter $AmtB_1$ because it is only expressed under N limitation (38) and is a key component under N limitation for transporting residual ammonium into the cell, which critically requires to be inhibited upon an upshift. To test this hypothesis, a pull-down experiment with purified C-terminal His_6-tag $AmtB_1$ was performed using crude cell extracts of *M. mazei* either grown under N limitation or under N limitation but shifted to ammonium sufficiency (0 → 10 mM) in an exponential growth phase for 30 min. After incubating $AmtB_1$-His_6 with 25 mg of the total cell extract, a Ni-NTA affinity chromatography was performed and the elution fractions were analyzed by SDS-PAGE and western blot using the anti-His tag and anti-sP36 antibodies. The results clearly show that exogenous $AmtB_1$-His_6 and native sP36 co-elute independent of the nitrogen conditions in which the cells were grown (Fig. 4). These findings strongly suggest that $AmtB_1$ forms a complex with sP36. The direct interaction between sP36 and $AmtB_1$ was further confirmed and evaluated by microscale thermophoresis (MST) using recombinant $AmtB_1$-His_6 and untagged sP36 (RED) resulting in an estimated dissociation constant of $K_D = 0.26 \pm 0.07$ µM (Fig. 5a).

As stated in the Introduction, in bacteria, the PII-like protein GlnK is known to interact with the ammonium transporter AmtB to modulate the transport activity of AmtB in

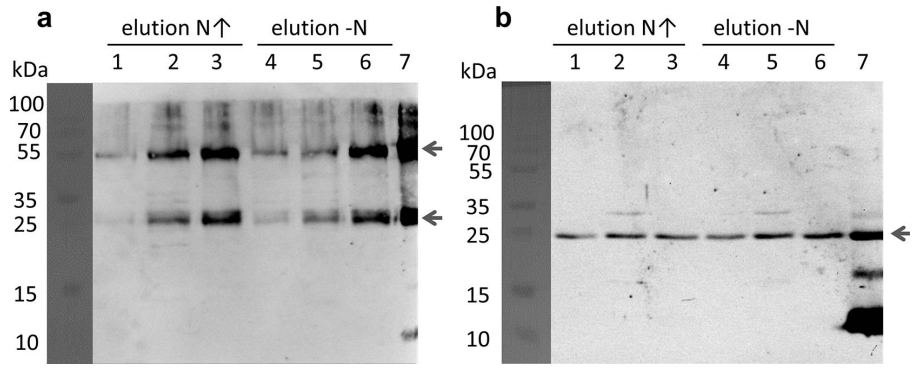

FIG 4 Pulldown with $AmtB_1$-His_6 as bait against *M. mazei* cell extract grown under N-limited (–N) and shifted to nitrogen-sufficient (N↑) condition. (a) Western blot using the anti-His-tag antibody shows $AmtB_1$ in the elution fractions of the N↑ and –N pulldowns. Indicated by a black arrow are the monomeric $AmtB_1$ at approximately 30 kDa and the dimeric $AmtB_1$ at 55 kDa. (b) Western blot with the specific sP36 peptide antibodies shows coelution of chromosomal-expressed native sP36 from the *M. mazei* cell extract with $AmtB_1$-His_6. 1–3: elutions of the pulldown using cell extract of cells grown under N upshift, 4–6: elutions of the pulldown using cell extract of cells grown under N-limited condition, 7: positive controls, purified $AmtB_1$-His_6 (a) and purified sP36 (b), respectively.

response to an ammonium upshift (52). Therefore, we next aimed to evaluate the interaction between sP36 and $GlnK_1$ by using recombinant N-terminal his-tagged $GlnK_1$ (His_6-$GlnK_1$) and sP36 (RED) proteins by MST, which yielded a dissociation constant of 1.8 ± 1.1 µM (Fig. 5b).

The interaction between sP36 and $GlnK_1$ was further verified by isothermal titration calorimetry (ITC, Fig. 5c). The ITC analysis clearly verified the interaction and demonstrated that sP36 forms a complex with $GlnK_1$ with a dissociation constant K_D of 5 µM in a 2:1 stoichiometry, that is, each monomer of $GlnK_1$ binds two sP36 monomers.

Given that $GlnK_1$ forms trimers in solution (27), a 2:1 stoichiometry aligns perfectly with the oligomeric state of sP36, which has been determined to form stable hexamers in solution by analytical size-exclusion chromatography (SEC) experiments. SEC was performed with sP36 from heterologous expression in *E. coli* as well as with His_6-sP36 purified from *M. mazei* (Fig. 6a and b). Using AlphaFold2 for computational modeling, we generated a structural model of hexameric sP36 (Fig. 6c), whose statistical parameters pLDDT and PAE (Fig. S2) demonstrate that the residues are correctly positioned in their local environment, and the monomers are accurately positioned relative to each other (50). The hexameric configuration of sP36 adopts a truncated cone shape, with the negative charged surface at the narrower side (Fig. 6d).

MST and ITC independently showed an interaction between sP36 and $GlnK_1$ with a high affinity (K_D in the low µM range). Thus, we next aimed at evaluating the impact of sP36 on the subcellular localization of $GlnK_1$. *M. mazei* wt and ΔsP36 strains were grown under N limitation followed by an ammonium upshift for 30 min, and the cultures were harvested in the mid-exponential growth phase. After subcellular fractionation, the presence of $GlnK_1$ was detected in the cytoplasmic and membrane fractions by western blot with specific antibodies. In the wt strain, $GlnK_1$ was predominantly present in the membrane fraction, while only a minor fraction was detected in the cytoplasm (Fig. 7). However, in ΔsP36, $GlnK_1$ is no longer detected in the membrane fraction, but mostly in the cytoplasm. In both subcellular fractions, $GlnK_1$ was detected at a different molecular weight, which corresponds to $GlnK_1$ in a stable complex with either soluble or membrane proteins. Remarkably, the total amount of $GlnK_1$ in the absence of sP36 appears to be decreased (Fig. 7a).

Since sP36 seems to be crucial for sequestration of $GlnK_1$ to the membrane, the interaction of $AmtB_1$ and $GlnK_1$ in dependence of sP36 was studied *in vitro*. In MST, AmtB1 (RED) only interacts with His_6-$GlnK_1$ if sP36 is present in the reaction buffer. If no sP36 was added to the reaction, no difference in MST traces was observed and no

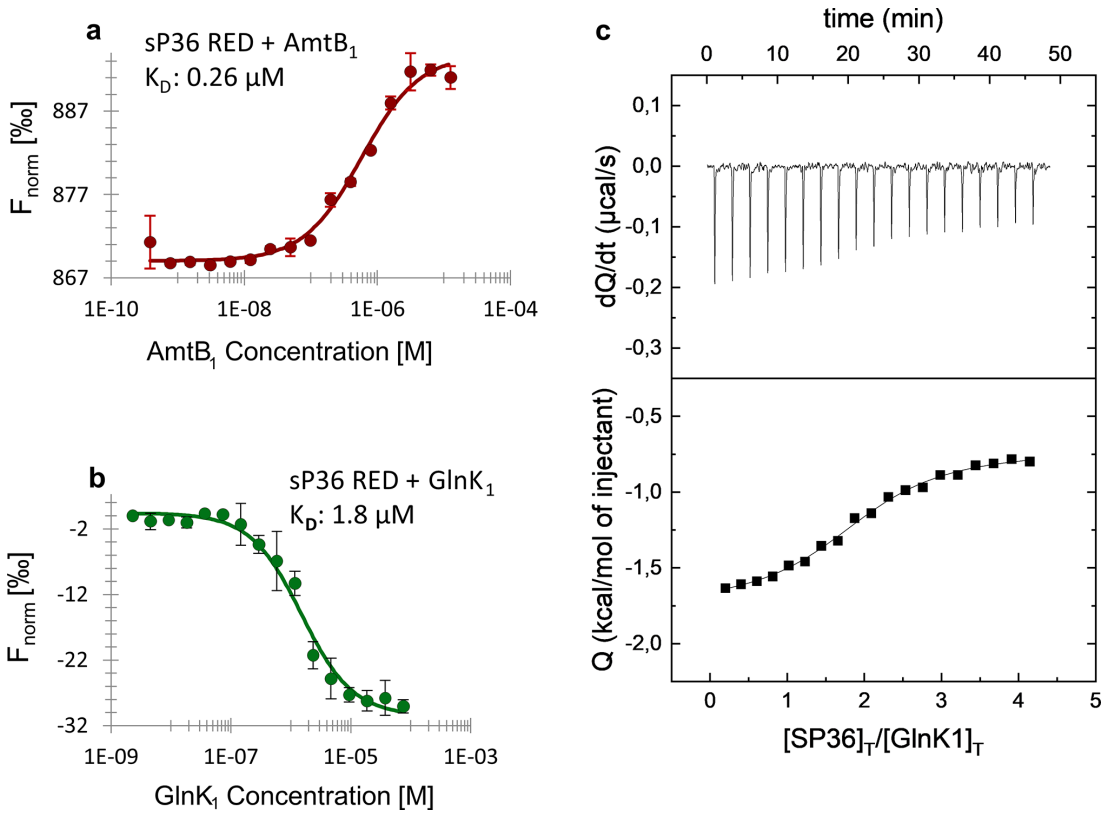

FIG 5 sP36 interaction studies using MST and isothermal titration calorimetry (ITC). (a) Interaction studies between sP36 and $AmtB_1$-His_6 using MST. RED-labeled untagged sP36 was used at 100 nM and $AmtB_1$-His_6 at different concentrations ranging from 12.5 µM to 0.38 nM, calculated based on the monomeric molecular mass. Based on three biological replicates, the K_D was estimated to be 0.26 µM (± 0.07 µM). (b) Interaction studies between sP36 and $GlnK_1$ using MST. RED-labeled untagged sP36 at 100 nM and His_6-$GlnK_1$ at 16 different concentrations ranging from 7.5 µM to 0.23 nM were used for MST analysis, resulting in a dissociation constant K_D of 1.8 µM (± 1.1 µM). In both cases (a and b), exemplarily one of the three biological replicates is depicted. (c) Interaction studies between sP36 and $GlnK_1$ using ITC. 20 µM His_6-$GlnK_1$ was titrated with 300 µM at 25°C. Control experiments were performed by injecting sP36 into buffer. The dissociation constant K_D was evaluated to be 5.4 µM. The sP36–$GlnK_1$ interaction has a stoichiometry of 2:1 as described in Materials and Methods.

interaction could be evaluated. However, in the presence of sP36, $AmtB_1$ interacts with $GlnK_1$ *in vitro* and a K_D of 7.7 µM was calculated (see Fig. 7b and c).

DISCUSSION

Based on the aforementioned results, we propose that in *M. mazei* both $GlnK_1$ and sP36 are required for the complete inhibition of $AmtB_1$, the ammonium transporter, in response to an upshift in ammonium concentration after a period of N limitation in *M. mazei*. The essential role of sP36 in $AmtB_1$ regulation during an N-upshift is further corroborated by our genetic analysis. The chromosomal mutant strain (*M. mazei* ΔsP36) displays a significantly prolonged lag phase when shifted from N limitation to ammonium sufficiency (10 mM NH_4^+) compared to the wild type strain. This strongly indicates that the ammonium transporter in the absence of sP36 retains significant activity, leading to an unnecessary cycle of active $AmtB_1$-mediated import together with passive diffusion, resulting in excessive energy consumption. This might explain the significantly prolonged lag phase observed in the deletion mutant strain after a shift to N sufficiency.

The mechanism of AmtB regulation by the PII protein GlnK is well characterized in *E. coli*. Here, the cellular nitrogen status is perceived by GlnD, which transduces the signal to GlnK through a covalent modification. Under N limitation, GlnK is uridylylated at the Y51 residue in the T-loop by GlnD. In response to increased ammonium concentrations, GlnK is rapidly deuridylylated by GlnD and the demodified GlnK subsequently interacts

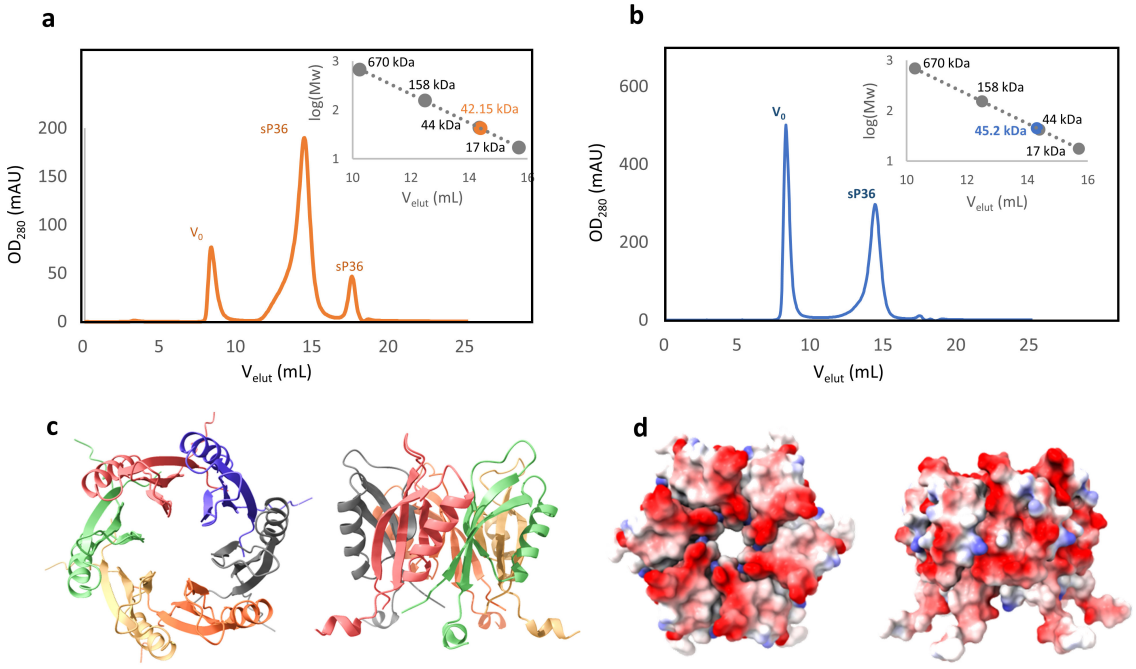

FIG 6 Oligomerization studies of purified sP36. (a) Untagged sP36 from expression in *E. coli*. Proteins and protein complexes were separated by SEC. The fractions of the main elution peak (retention volume of 14 mL to 15 mL) correspond to the molecular mass of the sP36 hexamer (42.6 kDa). Orange, sP36-His_6; gray, size-exclusion standard. (b) His_6-sP36 from expression in *M. mazei*. Proteins and protein complexes were separated in a SEC. The fractions of the main elution peak (retention volume of 14 mL to 15 mL) correspond to the molecular mass of the His_6-sP36 hexamer (47.8 kDa). Blue, sP36-His_6; gray, size-exclusion standard. (c and d) Structure prediction of a sP36 hexamer (50, 53). (c) Secondary structural elements of the sP36 hexamer, where each protomer is in a different color. (d) Electrostatic surface of the sP36 hexamer. The calculation was performed with the APBS plug-in implemented in PyMOL (Schrödinger Inc., 2015, The PyMOL Molecular Graphics System. Version 2.0 Schrödinger LLC). Color oscillates from −2.0 (red) to +2.0 (blue) KbT/ec.

with AmtB and inhibits its activity (46, 52). The trimeric GlnK binds AmtB with the T-loop of each monomer, physically blocking the hydrophobic pore of the AmtB trimer and the cytoplasmic pore exit (54). This regulatory mechanism appears to be highly conserved and has been also shown for *Rhodospirillum rubrum* (55), and the archaea *Haloferax mediterranei* (56, 57) and *Archaeoglobus fulgidus* (58). The *A. fulgidus* regulation was mainly proposed based on the structural studies of purified AmtB and by using a docking model for the interaction with the PII-like protein. Interestingly, the conserved T-loop of the *A. fulgidus* PII-like protein lacks the Y51 residue, which is the residue modified by uridylylation in *E. coli* (58).

In *M. mazei,* two copies of the *glnK*/*amtB* operon are present. While the $glnK_1/amtB_1$ operon is highly regulated in response to N availability by NrpR, the $amtB_2/glnK_2$ operon is not expressed under N limitation and has been proposed to be a potential backup system (38, 59). Although the T-loop of $GlnK_1$ contains the conserved tyrosine residue (Y51), no posttranslational modification of $GlnK_1$ could be observed in response to an ammonium upshift in *in vivo* and *in vitro* experiments (27). Moreover, no GlnD homolog is encoded in *M. mazei* (60) or in any archaeal genome. Consequently, in archaea like *M. mazei*, a potential $GlnK_1$ regulation of $AmtB_1$ requires a different mode of signal perception of changing nitrogen conditions.

Based on our results, we propose a hypothetical model for the regulation of $AmtB_1$ by sP36 in response to an increase in N availability, which is summarized in Fig. 8. In the absence of combined nitrogen or when the ammonium concentration is very low, most of the sP36 is located in the cytoplasm, while $AmtB_1$ actively transports the remaining NH_4^+ into the cell. When the external ammonium concentration increases (N-upshift), NH_3 diffusion provides the cell with sufficient ammonium. Thus, the energy-consuming

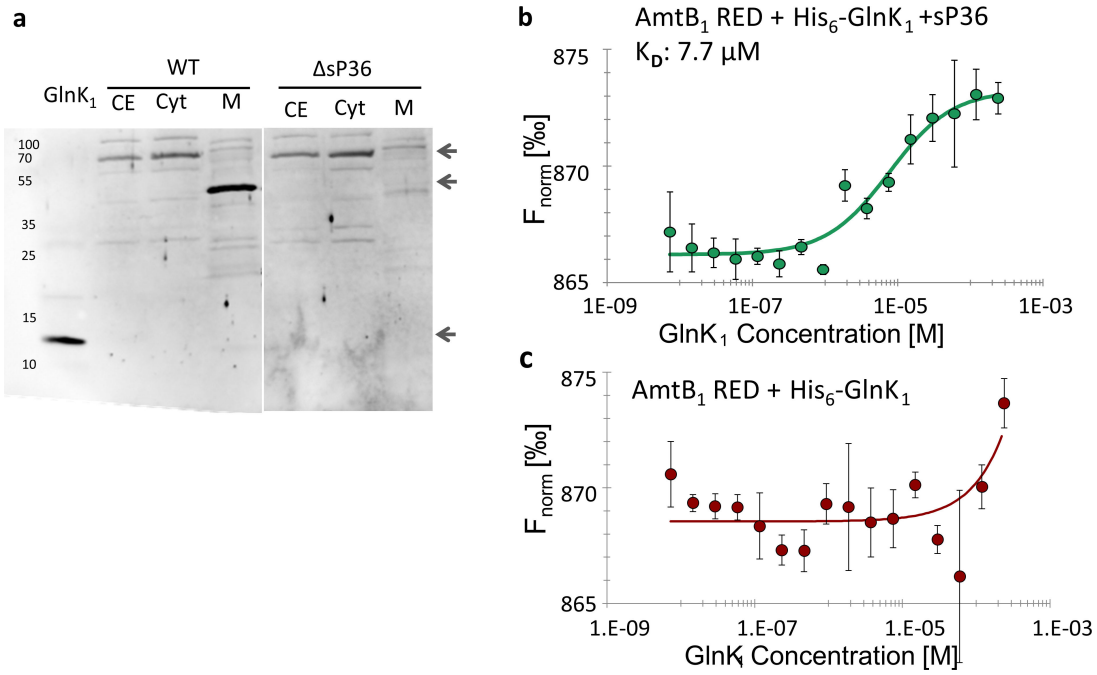

FIG 7 $AmtB_1$–$GlnK_1$ interaction is dependent on sP36. (a) Localization of $GlnK_1$ in *M. mazei* ΔsP36. *M. mazei* wt and ΔsP36 cultures (50 mL) were grown under N limitation until reaching the exponential growth phase and then shifted to N sufficiency (10 mM). Subcellular fractions were generated. The cell extract (CE) and cytoplasmic (Cyt) and membrane (M) fractions were evaluated for $GlnK_1$ presence by a western blot analysis using polyclonal antibodies against $GlnK_1$. Cyt and M fractions from *M. mazei* wt(DSM3647) and ΔsP36 were analyzed and compared to purified His_6-$GlnK_1$. The major $GlnK_1$ bands are indicated by arrows. Depicted is one exemplary western blot out of three biological replicates. (b and c) Interaction studies between $AmtB_1$-His_6 and $GlnK_1$-His_6 using MST. RED-labeled His_6-tagged $AmtB_1$ was used at 20 nM and $GlnK_1$-His_6 at different concentrations ranging from 480 µM to 14.6 nM, calculated based on the monomeric molecular mass. (b) In the presence of sP36 (480 µM), the K_D was estimated to be 7.7 µM (± 2.5 µM) based on three biological replicates. (c) In the absence of sP36, no interaction could be detected.

NH_4^+ transport by AmtB1 is inhibited through a direct protein–protein interaction with the $GlnK_1$ trimer. This complex formation between trimeric $AmtB_1$ and trimeric $GlnK_1$, however, is crucially dependent on hexameric sP36, which binds both proteins with high affinity. Consequently, sP36 favors the $AmtB_1$–$GlnK_1$ interaction in response to an ammonium upshift after a period of N limitation. The mechanism which triggers sP36 to interact with AmtB1 after ammonium upshift is still uncertain. However, most likely, oligomerization of sP36 is shifted toward a hexamer after an increase of ammonium concentration. This change is possibly based on sensing the concentration of 2-oxoglutarate and/or glutamine, which reflects the cell intern nitrogen availability. The nitrogen signal, the structure of the binary and ternary complexes, and the hierarchy of the interactions require further investigation and are currently being studied in our laboratory. We also note that the symmetry and the negatively charged surface on the sP36 hexamer (Fig. 6d) are well-suited to interact with the positively charged intracellular side of $AmtB_1$, as reported in the literature.

Finally, sP36 shows conservation in a broad range of methanogenic and halophilic archaea and is even present in the genome of some bacteria. It is worth noting that conservation of sP36 is coupled to an absence of the urydylyltransferase encoding *glnD*. Only a few bacteria also have a sP36 in addition to *glnD*. This might be due to horizontal gene transfer of the sP36 gene because those organisms are reported to grow in an highly diverse environment like animal intestinal tracts, also containing methanoarchaea. Consequently, the GlnD-dependent and the sP36-mediated pathways exhibit two different modes of AmtB regulation in separate groups of organisms. Due to the evolutionary placement of halophilic and methanogenic archaea, we speculate that sP36-mediated inhibition of $AmtB_1$ represents the archaeal, more ancient mechanism

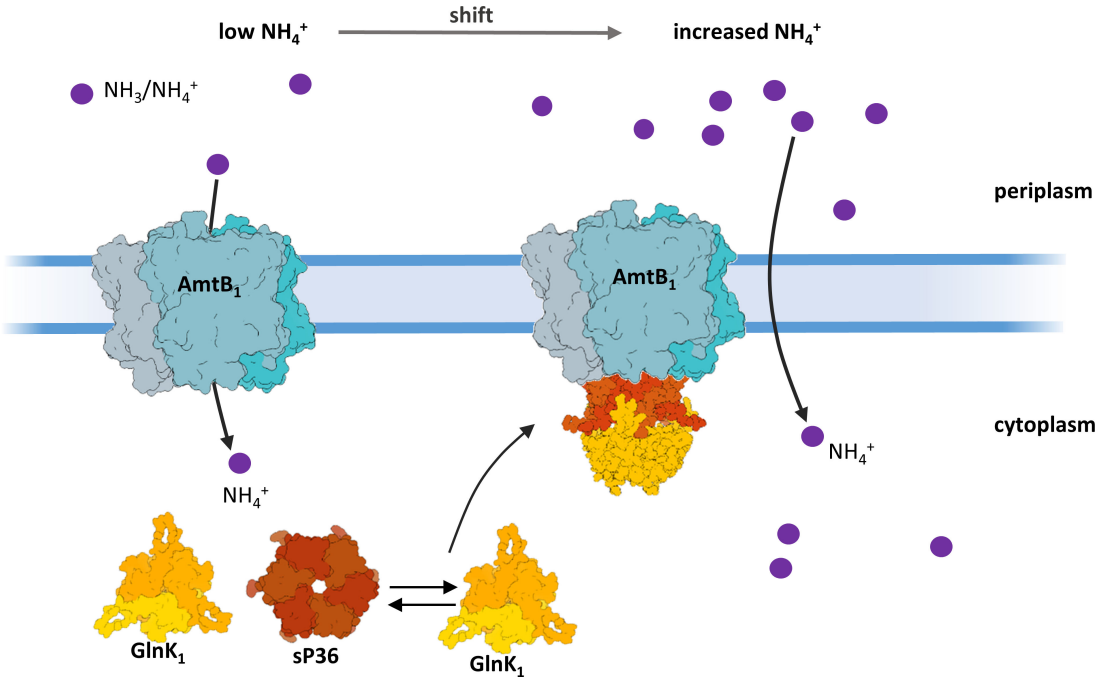

FIG 8 Hypothetical model of $AmtB_1$ regulation in *M. mazei*. The $AmtB_1$ trimer is actively importing ammonium under a low N concentration. However, after an upshift to ammonium sufficiency in the surrounding medium, sP36 is proposed to mediate the formation of a $GlnK_1$-$AmtB_1$ complex, allowing the $GlnK_1$ trimer to block the $AmtB_1$ activity to completeness. The displayed structures of GlnK1 and sP36 were generated using AlphaFold2 (50, 53) (Fig. S2). The structure of the ternary complex is a hypothetical model and requires further investigation.

for responding to changes in N availability, predating the AmtB inhibition by a PII-like protein, before the GlnD-dependent pathway evolved in bacteria.

MATERIALS AND METHODS

Construction of plasmids

sP36 genomic deletion

The flanking regions ~ 1,000 bp upstream and ~1,000 bp downstream of the sORF36 were amplified from genomic *M. mazei* DNA by using primers (Eurofins, Ebersberg, Germany) listed in Table S2. A puromycin resistance (Pur^R)-mediating *pac*-cassette was restricted from pRS207. The 1,000 bp downstream fragment was restricted by enzymes *EcoRI* and *BamHI* and inserted into the multiple cloning site (MCS) of the vector pMCL210, resulting in pRS1305. The 1,000 bp upstream fragment was cleaved using *EcoRI* and *KpnI* and subsequently ligated in pRS1305. The resulting plasmid was designated pRS1307. The *pac*-cassette was ligated into the *EcoRI* site of pRS1307 and the resulting plasmid was named pRS1308. pRS1308 was linearized using *ScaI* and transformed into *M. mazei* wt (3A) cells by liposome-mediated transformation. Insertion in the chromosome occurred through double homologous recombination by selection for puromycin resistance[57]. The success of the allelic marker exchange of single-mutant colonies was verified in puromycin-containing media and further analyzed via Southern blot analysis with specific probes directed against the *sP36* gene and *pac*-cassette (Fig. S1).

sP36 overexpression

For cloning *MMsORF36* into pETSUMO, pET28a, and pWM321, a construct including the *pmcrB* promotor and $(His)_6$-*MMsORF36* fusion was synthesized (Eurofins Genomics, Ebersberg, Germany). The plasmid was named pRS1214. *MMsORF36* was cloned into

pETSUMO using pRS1214 as a template, primer pair sORF36_3for/sORF36_3rev, and the Champion pET SUMO expression system (Thermo Fisher Scientific, Waltham, USA) according to the manufacturer's instructions, yielding plasmid pRS1240 and strain *E. coli* BL21 K4099. The cloning of *MMsORF36* into pET28a was done via an intermediate. First, *MMsORF36* was amplified with the primer pair sORF36_forNdeI/sORF36_3revNdeI (Table S2) using the template pRS1214 and subsequently ligated via TA cloning into the pCRII vector (Thermo Fisher Scientific, Waltham, USA) according to the manufacturer's instructions. The resulting construct was designated pRS1223 in *E. coli* DH5α K4071. In the second step, the insert was excised from pRS1223 using the *NdeI* site and ligated into the *NdeI* site of pET28a. The resulting plasmid was designated pRS1225 and transformed in *E. coli* BL21 pRIL yielding the strain K4092. Upon cloning of *MMsORF36* in pWM321, the *pmcrB* promotor-$(His)_6$-*MMsORF36* fusion was isolated using *SacI* and *KpnI* sites from pRS1214 and ligated into the corresponding sites of pWM321, resulting in plasmid pRS1227. pRS1227 was transformed into *M. mazei* wt (3A) as described before (53).

His_5-SUMO-TEV-sP36 construct

A TEV (tobacco etch virus protease) cleavage site was inserted between the Sumo tag and sORF36 in the His_5-SUMO-sP36 overexpression construct (pRS1240). Therefore, site-directed mutagenesis was conducted using primers SP36_TEV_rv and SP36_TEV_fw (Table S2).

Growth of *M. mazei*

M. mazei was cultivated in sealed bottles of an anaerobic minimal medium with a gaseous phase consisting of N_2 and CO_2 (vol/vol, 80/20) (26, 60). The medium was supplemented with 150 mM methanol as carbon source, and in case of cultures growing in nitrogen sufficiency, additionally 10 mM ammonium chloride was used. Cells were cultivated until an optical turbidity of 0.5–0.6 at 600 nm (T_{600} = 0.5–0.6). –N Cells were grown until T_{600} = 0.2–0.3.

M. mazei cells were harvested by centrifugation at 4,000 *g* at 4°C for 30 min. The cells were resuspended in 2 mL of 50 mM Tris buffer (pH 7.6) and lysed by using a dismembrator (Sartorius, Göttingen, Germany) at 1,600 rpm for 3 min. The whole cell extract was centrifuged for 30 min at 13,000 *g* and 4°C to get rid of cell debris and the remaining unlysed cells.

Subcellular fractionation

For subcellular fractionation of *M. mazei*, the cultures were grown anaerobically as described. Cells were harvested by centrifugation t 6,000 *g* at 4°C for 30 min. The cells were resuspended in 10 mL of Tris buffer (50 mM, pH 7.6) and afterward lysed by using a dismembrator (Sartorius, Göttingen, Germany) at 1,600 rpm for 3 min. The lysate was centrifuged for 30 min at 7,500 *g* and 4°C. To separate the membrane and cytoplasmic fractions, the supernatant was further centrifuged at 210,000 *g* for 1 h at 4°C.

Purification of expressed proteins

His_6-sP36, His_6-GlnK1, and His_6-SUMO-sP36

E. coli Bl21 (DE3)/pRIL cultures were grown in an LB (Luria-Bertani) medium at 37°C under continuous shaking. At T_{600} = 0.6, the protein expression was induced by adding 100 µM IPTG (isopropyl-β-thiogalactoside) (final concentration) and the cultures were incubated for 2 hours. Cells were harvested by centrifugation at 4,000 *g* at 4°C for 20 min, suspended in 6 mL of phosphate buffer A (50 mM phosphate, 300 mM NaCl, pH 8.0) and lysed by passing through a French pressure cell two times with 80 $N(mm^2)^{-1}$. Afterward. the extract was centrifuged for 30 min at 13,000 *g* and 4°C to get rid of cell debris and the remaining unlysed cells. For protein purification from *M. mazei*, cultures were grown and lysed as described above. His-tagged proteins were purified by affinity chromatography

on Ni-NTA agarose (Qiagen, Hilden, Germany) gravity flow columns with 1 mL of bed volume. Proteins were eluted in steps with 100 mM, 250 mM, and 500 mM imidazole.

SUMO cleavage

For cleavage of the SUMO-$(His)_6$-tag, 200 µL of SUMO-protease (Thermo Fisher Scientific, Waltham, MA, USA) per 1 mg of tagged protein was used. The reaction mixture was incubated for 1 h at 30°C. The cleaved sP36 protein was afterward purified by a second step of affinity using Ni-NTA agarose (Qiagen, Hilden, Germany) in phosphate buffer A.

His_5-SUMO-TEV-sP36 construct

E. coli Rosetta containing the His_5-SUMO-TEV-sP36 construct was grown in the LB medium at 37°C under continuous shaking. At T_{600} = 0.6, the protein expression was induced by adding 100 µM IPTG (final concentration) and the cultures were incubated over night at 20°C. Cells were harvested by centrifugation at 4,000 *g* at 4°C for 20 min, suspended in the Tris-HCl buffer A (20 mM Tris-HCl, 300 mM NaCl, pH 8.0), and lysed by sonication (Gardiner, NY, USA). Afterward, the extract was centrifuged for 30 min at 13,000 *g* and 4°C. His-tagged proteins were purified by affinity chromatography in a HisTrap column (Cytiva, Marlborough, MA, USA). Proteins were eluted with the Tris-HCl buffer with 500 mM imidazole. Protein fractions were dialyzed against 20 mM Tris-HCl, 0.5 M NaCl, 2 mM DTT, pH 8.0 in the presence of TEV protease. The cleaved sP36 protein was afterward separated from undigested tagged sP36, cleaved His_5-SUMO-TEV-tag, as well as the His-tagged TEV protease by a second step of affinity using a HisTrap column (Cytiva, Marlborough, MA, USA). Final purification was conducted using gel filtration with a S-100 Sephacryl HR column (Cytiva, Marlborough, MA, USA) and 20 mM Tris-HCl, pH 8.0, 0.15 M NaCl buffer.

$AmtB_1$-His_6

$AmtB_1$-His_6 was purified from heterologous overexpression in *E. coli* C43 using a solubilized membrane fraction. Therefore, cultures were grown in the LB medium at 37°C. At T_{600} = 0.6, the protein expression was induced by adding 500 µM IPTG (final concentration) and the cultures were incubated for 3 hours at 37°C. Cells were harvested by centrifugation at 6,000 *g* for 20 min at 4°C. Next, a 4 g pellet was resuspended in 4 mL of 50 mM Tris buffer (pH 7.6) and lysed by passing through the French pressure cell two times at 40 $N(mm^2)^{-1}$. The extract was then centrifuged again at 8,000 *g* for 20 min at 4°C to remove the remaining unlysed cells and cell debris. The cleared supernatant was transferred into new tubes and centrifuged in an ultracentrifuge (Optima XPN-100 Ultracentrifuge, Beckman Coulter, Brea, California, USA) for 1 h at 210,000 *g* and 4°C. The membrane pellet was washed with 15 mL of 50 mM Tris buffer (pH 7.6) and again centrifuged in the ultracentrifuge for 1 h at 4°C and 210,000 *g*. Afterward, the membrane proteins in the pellet were solubilized in 1 mL of phosphate buffer B (50 mM phosphate, 150 mM NaCl, 2% DDM, pH 8.0).

The solubilized membrane fraction was added on an affinity chromatography Co-NTA agarose gravity flow column (bed volume: 0.5 mL). For washing and elution steps, phosphate buffer C (50 mM phosphate, 150 mM NaCl, 0.05% DDM, pH 8.0) was used. His-tagged proteins were eluted in 0.5 mL steps using phosphate buffer C with 100 mM, 250 mM, and 500 mM imidazole.

MST

Proteins were purified to apparent homogeneity by affinity chromatography using Ni-NTA agarose and labeled with the RED-NHS, 2nd generation, 650 nm fluorescent dye using the Monolith NT RED-NHS lysine labeling kit according to manufacturer's protocol (NanoTemper, Munich, Germany). RED-labeled untagged sP36 at 100 nM and His6-GlnK1 at 16 different concentrations ranging from 7.5 µM to 0.23 nM or 10 nM of sP36-RED and $AmtB_1$-His_6 in 16 dilutions ranging from 12.6 µM to 0.38 nM (all concentrations

based on monomeric molecular mass) were used. The protein interaction was measured in standard capillaries (NanoTemper), 100% excitation power, and medium or high MST power (IR laser intensity). Both interactions were tested in three biological replicates. For measuring the interaction between $AmtB_1$ and $GlnK_1$ in dependence of sP36, RED-labeled His_6-$AmtB_1$ at 20 nM and $GlnK_1$ at 16 different concentrations ranging from 480 µM to 14.6 nM and untagged purified sP36 at 480 µM or 0 µM (concentrations based on the monomeric molecular weight) were used. The protein interaction was measured in standard capillaries (NanoTemper), 20% excitation power, and medium MST power (IR laser intensity). Interactions were tested in three biological replicates.

ITC

Standard ITC experiments were performed using an Auto-iTC200 system (MicroCal, Malvern Panalytical, Malvern, UK). Briefly, 20 µM GlnK1 was titrated with 300 µM sP36 in a buffer of 100 mM potassium phosphate, 2 mM EDTA, pH 7.0 at 25°C. Control experiments were performed by injecting the sP36 protein into the buffer. The heats of dilution were negligible. The resulting heats were integrated and normalized by ligand injected and fitted with a model for a single ligand binding site implemented in the software package Origin 7.0 (OriginLab Corporation, Northampton, MA, USA) employing user-defined fitting routines.

SEC

SEC was conducted with 0.3 mg of His_6-sP36, purified from homologous expression in *M. mazei,* and 0.5 mg of untagged sP36 (derived from His_6-SUMO-sP36) using 50 mM phosphate buffer containing 300 mM NaCl and the analytical gel filtration column ENrich SEC 650 (BioRad, Hercules, USA). The protein was eluted at a flow rate of 1 mL min^{-1} with 50 mM phosphate buffer (150 mM NaCl, pH 8.0). Elutions were collected in 1 mL fractions. In order to calibrate the chromatograph, a protein mix (BioRad size-exclusion standard; #151–1901, BioRad, Hercules, USA) was used as a standard.

AUTHOR AFFILIATIONS

[1]Institut für allgemeine Mikrobiologie, Christian-Albrechts-Universität zu Kiel, Kiel, Germany
[2]Institute of Biocomputation and Physics of Complex Systems (BIFI), Universidad de Zaragoza, Zaragoza, Spain
[3]Departamento de Bioquímica y Biología Molecular y Celular, Universidad de Zaragoza, Zaragoza, Spain
[4]Instituto de Investigaciones Sanitarias de Aragón (IIS Aragón), Zaragoza, Spain
[5]Centro de Investigación Biomédica en Red de Enfermedades Hepáticas y Digestivas (CIBEREHD), Madrid, Spain
[6]Departamento de Microbiología y Genética, Universidad de Salamanca, Salamanca, Spain
[7]Instituto de Recursos Naturales y Agrobiología de Salamanca, Spanish National Research Council (IRNASA-CSIC), Salamanca, Spain

AUTHOR ORCIDs

Tim Habenicht http://orcid.org/0009-0004-1237-6299
Katrin Weidenbach http://orcid.org/0000-0003-1544-2031
Ruben M. Buey http://orcid.org/0000-0003-1263-0221
Ruth A. Schmitz http://orcid.org/0000-0002-6788-0829

FUNDING

Funder	Grant(s)	Author(s)
Deutsche Forschungsgemeinschaft (DFG)	SCHM1052/20-1+2	Katrin Weidenbach Ruth A. Schmitz Tim Habenicht
MEC | Agencia Estatal de Investigación (AEI)	PID2019-110900GB-I00	Monica Balsera

AUTHOR CONTRIBUTIONS

Tim Habenicht, Conceptualization, Formal analysis, Investigation, Methodology, Visualization, Writing – original draft, Writing – review and editing | Katrin Weidenbach, Conceptualization, Supervision, Writing – review and editing | Adrian Velazquez-Campoy, Investigation, Methodology, Writing – review and editing | Ruben M. Buey, Methodology, Writing – review and editing | Monica Balsera, Methodology, Writing – review and editing | Ruth A. Schmitz, Conceptualization, Formal analysis, Funding acquisition, Methodology, Resources, Supervision, Validation, Writing – review and editing

ADDITIONAL FILES

The following material is available online.

Supplemental Material

Fig. S1 (Spectrum02811-23-S0001.tif). Southern blot of *M. mazei* Δsp36 genomic DNA: to test the success of the sp36 deletion in *M. mazei.*
Fig. S2 (Spectrum02811-23-S0002.tif). Confidence of the predicted structure of sP36.
Fig. S3 (Spectrum02811-23-S0003.tif). Color-coded representation of the electrostatic potential of the surface of AmtB1 and sP36.
Table S1 (Spectrum02811-23-S0004.docx). Strains and plasmids used.
Table S2 (Spectrum02811-23-S0005.docx). Oligonucleotides used.

REFERENCES

1. Weidenbach K, Gutt M, Cassidy L, Chibani C, Schmitz RA. 2022. Small proteins in archaea, a mainly unexplored world. J Bacteriol 204:e0031321. https://doi.org/10.1128/JB.00313-21
2. Ramamurthi KS, Storz G. 2014. The small protein floodgates are opening; now the functional analysis begins. BMC Biol 12:96. https://doi.org/10.1186/s12915-014-0096-y
3. Storz G, Wolf YI, Ramamurthi KS. 2014. Small proteins can no longer be ignored. Annu Rev Biochem 83:753–777. https://doi.org/10.1146/annurev-biochem-070611-102400
4. Steinberg R, Koch HG. 2021. The largely unexplored biology of small proteins in pro- and eukaryotes. FEBS J 288:7002–7024. https://doi.org/10.1111/febs.15845
5. Basrai MA, Hieter P, Boeke JD. 1997. Small open reading frames: beautiful needles in the haystack. Genome Res 7:768–771. https://doi.org/10.1101/gr.7.8.768
6. Angiuoli SV, Gussman A, Klimke W, Cochrane G, Field D, Garrity GM, Kodira CD, Kyrpides N, Madupu R, Markowitz V, Tatusova T, Thomson N, White O. 2008. Toward an online repository of standard operating procedures (Sops) for (Meta) genomic annotation. OMICS 12:137–141. https://doi.org/10.1089/omi.2008.0017
7. Tatusova T, DiCuccio M, Badretdin A, Chetvernin V, Nawrocki EP, Zaslavsky L, Lomsadze A, Pruitt KD, Borodovsky M, Ostell J. 2016. NCBI prokaryotic genome annotation pipeline. Nucleic Acids Res 44:6614–6624. https://doi.org/10.1093/nar/gkw569
8. Steen H, Mann M. 2004. The ABC's (and Xyz's) of peptide sequencing. Nat Rev Mol CELL Biol 5:699–711. https://doi.org/10.1038/nrm1468
9. Ahrens CH, Wade JT, Champion MM, Langer JD. 2022. A practical guide to small protein discovery and characterization using mass spectrometry. J Bacteriol 204:e0035321. https://doi.org/10.1128/JB.00353-21
10. Jäger D, Sharma CM, Thomsen J, Ehlers C, Vogel J, Schmitz RA. 2009. Deep sequencing analysis of the *Methanosarcina mazei* Goe1 transcriptome in response to nitrogen availability . Proc. Natl. Acad. Sci. U.S.A 106:21878–21882. https://doi.org/10.1073/pnas.0909051106
11. Kaulich PT, Cassidy L, Bartel J, Schmitz RA, Tholey A. 2021. Multi-protease approach for the improved identification and molecular characterization of small proteins and short open reading frame-encoded peptides. J Proteome Res 20:2895–2903. https://doi.org/10.1021/acs.jproteome.1c00115
12. Vazquez-Laslop N, Sharma CM, Mankin A, Buskirk AR. 2022. Identifying small open reading frames in prokaryotes with ribosome profiling. J Bacteriol 204:e0029421. https://doi.org/10.1128/JB.00294-21
13. Hadjeras L, Bartel J, Maier L-K, Maaß S, Vogel V, Svensson SL, Eggenhofer F, Gelhausen R, Müller T, Alkhnbashi OS, Backofen R, Becher D, Sharma CM, Marchfelder A. 2023. Revealing the small proteome of *Haloferax volcanii* by combining ribosome profiling and small-protein optimized mass spectrometry. Microlife 4:uqad001. https://doi.org/10.1093/femsml/uqad001
14. Cassidy L, Kaulich PT, Maaß S, Bartel J, Becher D, Tholey A. 2021. Bottom-up and top-down proteomic approaches for the identification, characterization, and quantification of the low molecular weight proteome with focus on short open reading frame-encoded peptides. Proteomics 21:e2100008. https://doi.org/10.1002/pmic.202100008
15. Orr MW, Mao Y, Storz G, Qian SB. 2020. Alternative ORFs and small ORFs: shedding light on the dark proteome. Nucleic Acids Res 48:1029–1042. https://doi.org/10.1093/nar/gkz734

16. Gray T, Storz G, Papenfort KSP. 2022. Small proteins; big questions. J Bacteriol 204:e0034121. https://doi.org/10.1128/JB.00341-21
17. Weaver J, Mohammad F, Buskirk AR, Storz G. 2019. Identifying small proteins by ribosome profiling with stalled initiation complexes. mBio 10:e02819-18. https://doi.org/10.1128/mBio.02819-18
18. Hemm MR, Weaver J, Storz G. 2020. Escherichia coli small Proteome. EcoSal Plus 9. https://doi.org/10.1128/ecosalplus.ESP-0031-2019
19. Lloyd CR, Park S, Fei J, Vanderpool CK. 2017. The small protein SgrT controls transport activity of the glucose-specific phosphotransferase system. J Bacteriol 199:e00869-16. https://doi.org/10.1128/JB.00869-16
20. Gutt M, Jordan B, Weidenbach K, Gudzuhn M, Kiessling C, Cassidy L, Helbig A, Tholey A, Pyper DJ, Kubatova N, Schwalbe H, Schmitz RA. 2021. High complexity of glutamine synthetase regulation in *Methanosarcina mazei*: small protein 26 interacts and enhances glutamine synthetase activity. FEBS J 288:5350–5373. https://doi.org/10.1111/febs.15799
21. Zahn S, Kubatova N, Pyper DJ, Cassidy L, Saxena K, Tholey A, Schwalbe H, Soppa J. 2021. Biological functions, genetic and biochemical characterization, and NMR structure determination of the small zinc finger protein Hvo_2753 from *Haloferax volcanii* . The FEBS Journal 288:2042–2062. https://doi.org/10.1111/febs.15559
22. van Wolferen M, Wagner A, van der Does C, Albers S-V. 2016. The archaeal Ced system imports DNA. Proc Natl Acad Sci U S A 113:2496–2501. https://doi.org/10.1073/pnas.1513740113
23. Egea PF, Stroud RM. 2010. Lateral opening of a translocon upon entry of protein suggests the mechanism of insertion into membranes. Proc Natl Acad Sci U S A 107:17182–17187. https://doi.org/10.1073/pnas.1012556107
24. Hippe H, Caspari D, Fiebig K, Gottschalk G. 1979. Utilization of trimethylamine and other N methyl compounds for growth and methane formation by Methanosarcina barkeri. Proc Natl Acad Sci U S A 76:494–498. https://doi.org/10.1073/pnas.76.1.494
25. Deppenmeier U, Müller V, Gottschalk G. 1996. Pathways of energy conservation in methanogenic archaea. Arch. Microbiol 165:149–163. https://doi.org/10.1007/BF01692856
26. Ehlers Claudia, Veit K, Gottschalk G, Schmitz RA. 2002. Functional organization of a single Nif cluster in the mesophilic archaeon *Methanosarcina mazei* strain Gö1. Archaea 1:143–150. https://doi.org/10.1155/2002/362813
27. Ehlers C., Grabbe R, Veit K, Schmitz RA. 2002. Erratum: characterization of G1Nk1 from *Methanosarcina mazei* strain Goe1: complementation of an *Escherichia coli* glnK mutant strain by G1Nk1. J Bacteriol 184:1028–1040. https://doi.org/10.1128/jb.184.4.1028-1040.2002
28. Weidenbach K, Ehlers C, Kock J, Ehrenreich A, Schmitz RA. 2008. Insights into the NrpR regulon in *Methanosarcina mazei* Gö1. Arch Microbiol 190:319–332. https://doi.org/10.1007/s00203-008-0369-3
29. Weidenbach K, Ehlers C, Kock J, Schmitz RA. 2010. NrpRII mediates contacts between NrpRI and general transcription factors in the archaeon *Methanosarcina mazei* Gö1. FEBS J 277:4398–4411. https://doi.org/10.1111/j.1742-4658.2010.07821.x
30. Weidenbach K, Ehlers C, Schmitz RA. 2014. The transcriptional activator NrpA is crucial for inducing nitrogen fixation in *Methanosarcina mazei* Gö1 under nitrogen-limited conditions. FEBS J 281:3507–3522. https://doi.org/10.1111/febs.12876
31. Prasse Daniela, Thomsen J, De Santis R, Muntel J, Becher D, Schmitz RA. 2015. First description of small proteins encoded by spRNAs in *Methanosarcina mazei* strain Gö1. Biochimie 117:138–148. https://doi.org/10.1016/j.biochi.2015.04.007
32. Leigh JA, Dodsworth JA. 2007. Nitrogen regulation in bacteria and archaea. Annu Rev Microbiol 61:349–377. https://doi.org/10.1146/annurev.micro.61.080706.093409
33. Prasse D., Förstner KU, Jäger D, Backofen R, Schmitz RA. 2017. RNA biology sRNA 154 a newly identified regulator of nitrogen fixation in *Methanosarcina mazei* strain Gö1. RNA Biol 14:1544–1558. https://doi.org/10.1080/15476286.2017.1306170
34. Zimmer DP, Soupene E, Lee HL, Wendisch VF, Khodursky AB, Peter BJ, Bender RA, Kustu S. 2000. Nitrogen regulatory protein C-controlled genes of *Escherichia coli*: scavenging as a defense against nitrogen limitation. Proc Natl Acad Sci U S A 97:14674–14679. https://doi.org/10.1073/pnas.97.26.14674
35. Magasanik B, Kaiser CA. 2002. Nitrogen regulation in *Saccharomyces cerevisiae*. Gene 290:1–18. https://doi.org/10.1016/s0378-1119(02)00558-9
36. Halbleib CM, Ludden PW. 2000. Regulation of biological nitrogen fixation. J Nutr 130:1081–1084. https://doi.org/10.1093/jn/130.5.1081
37. Brill WJ. 1975. Regulation and genetics of bacterial nitrogen fixation. Annu Rev Microbiol 29:109–129. https://doi.org/10.1146/annurev.mi.29.100175.000545
38. Veit K, Ehlers C, Ehrenreich A, Salmon K, Hovey R, Gunsalus RP, Deppenmeier U, Schmitz RA. 2006. Global transcriptional analysis of *Methanosarcina mazei* strain Gö1 under different nitrogen availabilities. Mol Genet Genomics 276:41–55. https://doi.org/10.1007/s00438-006-0117-9
39. Boogerd FC, Ma H, Bruggeman FJ, van Heeswijk WC, García-Contreras R, Molenaar D, Krab K, Westerhoff HV. 2011. AmtB-mediated NH_3 transport in prokaryotes must be active and as a consequence regulation of transport by GlnK is mandatory to limit futile Cycling of Nh4(+)/Nh3. FEBS Lett 585:23–28. https://doi.org/10.1016/j.febslet.2010.11.055
40. Wacker T, Garcia-Celma JJ, Lewe P, Andrade SLA. 2014. Direct observation of electrogenic NH_4+ transport in ammonium transport (AMT) proteins. Proc Natl Acad Sci U S A 111:9995–10000. https://doi.org/10.1073/pnas.1406409111
41. Ehlers C, Weidenbach K, Veit K, Forchhammer K, Schmitz RA. 2005. Unique mechanistic features of post-translational regulation of glutamine synthetase activity in *Methanosarcina mazei* strain Gö1 in response to nitrogen availability. Mol Microbiol 55:1841–1854. https://doi.org/10.1111/j.1365-2958.2005.04511.x
42. Marini A-M, Urrestarazu A, Beauwens R, André B. 1997. The Rh (Rhesus) blood group polypeptides are related to NH_4 transporters. Trends Biochem Sci 22:460–461. https://doi.org/10.1016/s0968-0004(97)01132-8
43. Thomas GH, Mullins JGL, Merrick M. 2000. Membrane topology of the MEP/AMT family of ammonium transporters. Mol Microbiol 37:331–344. https://doi.org/10.1046/j.1365-2958.2000.01994.x
44. Khademi S, O'Connell J 3rd, Remis J, Robles-Colmenares Y, Miercke LJW, Stroud RM. 2004. Mechanism of ammonia transport by AMT/MEP/Rh: Structure of AmtB at 135 Å. Science 305:1587–1594. https://doi.org/10.1126/science.1101952
45. Zheng L, Kostrewa D, Bernèche S, Winkler FK, Li XD. 2004. The mechanism of ammonia transport based on the crystal structure of AmtB of *Escherichia coli*. Proc Natl Acad Sci U S A 101:17090–17095. https://doi.org/10.1073/pnas.0406475101
46. Coutts G, Thomas G, Blakey D, Merrick M. 2002. Membrane sequestration of the signal transduction protein GlnK by the ammonium transporter AmtB. EMBO J 21:536–545. https://doi.org/10.1093/emboj/21.4.536
47. Atkinson MR, Ninfa AJ. 1998. Role of the GlnK signal transduction protein in the regulation of nitrogen assimilation in *Escherichia Coli*. Mol Microbiol 29:431–447. https://doi.org/10.1046/j.1365-2958.1998.00932.x
48. Thomas G, Coutts G, Merrick M. 2000. The glnKamtB operon. A conserved gene pair in prokaryotes. Trends Genet 16:11–14. https://doi.org/10.1016/s0168-9525(99)01887-9
49. Altschul SF, Gish W, Miller W, Myers EW, Lipman DJ. 1990. Basic local alignment search tool. Journal of molecular biology 215:403–410. https://doi.org/10.1016/S0022-2836(05)80360-2
50. Jumper J, Evans R, Pritzel A, Green T, Figurnov M, Ronneberger O, Tunyasuvunakool K, Bates R, Žídek A, Potapenko A, et al. 2021. Highly accurate protein structure prediction with Alphafold. Nature 596:583–589. https://doi.org/10.1038/s41586-021-03819-2
51. Parks DH, Chuvochina M, Rinke C, Mussig AJ, Chaumeil P-A, Hugenholtz P. 2022. GTDB: An ongoing census of bacterial and Archaeal diversity through a Phylogenetically consistent, rank normalized and complete genome-based Taxonomy. Nucleic acids research 50:D785–D794. https://doi.org/10.1093/nar/gkab776
52. Javelle A, Severi E, Thornton J, Merrick M. 2004. Ammonium sensing in *Escherichia coli*: role of the ammonium transporter AmtB and AmtB-GlnK complex formation. J Biol Chem 279:8530–8538. https://doi.org/10.1074/jbc.M312399200
53. Mirdita M, Schütze K, Moriwaki Y, Heo L, Ovchinnikov S, Steinegger M. 2022. Brief communication colabfold: making protein folding accessible to all. Nat Methods 19:679–682. https://doi.org/10.1038/s41592-022-01488-1

54. Conroy MJ, Durand A, Lupo D, Li X-D, Bullough PA, Winkler FK, Merrick M. 2007. The crystal structure of the *Escherichia coli* AmtB-GlnK complex reveals how GlnK regulates the ammonia channel. Proc Natl Acad Sci U S A 104:1213–1218. https://doi.org/10.1073/pnas.0610348104
55. Jonsson A, Nordlund S. 2007. *In vitro* studies of the uridylylation of the three P_{II} protein paralogs from *Rhodospirillum rubrum*: the transferase activity of *R. rubrum* GlnD is regulated by α-Ketoglutarate and divalent cations but not by glutamine . J Bacteriol 189:3471–3478. https://doi.org/10.1128/JB.01704-06
56. Pedro-Roig Laia, Camacho M, Bonete MJ. 2013. Haloferax mediterranei GlnK proteins are post-translationally modified by uridylylation. Proteomics 13:1371–1374. https://doi.org/10.1002/pmic.201200465
57. Pedro-Roig L., Lange C, Bonete MJ, Soppa J, Maupin-Furlow J. 2013. Nitrogen regulation of protein-protein interactions and transcript levels of GlnK P_{II} regulator and AmtB ammonium transporter homologs in archaea. Microbiologyopen 2:826–840. https://doi.org/10.1002/mbo3.120
58. Andrade SLA, Dickmanns A, Ficner R, Einsle O. 2005. Crystal structure of the archaeal ammonium transporter Amt-1 from *Archaeoglobus fulgidus*. Proc Natl Acad Sci U S A 102:14994–14999. https://doi.org/10.1073/pnas.0506254102
59. Ehlers C, Weidenbach K, Veit K, Deppenmeier U, Metcalf WW, Schmitz RA. 2005. Development of genetic methods and construction of a chromosomal GlnK 1 mutant in *Methanosarcina mazei* strain Gö1. Mol Genet Genomics 273:290–298. https://doi.org/10.1007/s00438-005-1128-7
60. Deppenmeier U, Johann A, Hartsch T, Merkl R, Schmitz RA, Martinez-Arias R, Henne A, Wiezer A, Bäumer S, Jacobi C, Brüggemann H, Lienard T, Christmann A, Bömeke M, Steckel S, Bhattacharyya A, Lykidis A, Overbeek R, Klenk H-P, Gunsalus RP, Fritz H-J, Gottschalk G. 2002. The genome of *Methanosarcina mazei*: evidence for lateral gene transfer between bacteria and archaea. J Mol Microbiol Biotechnol 4:453–461.